

CAM-VFD: Cross-Attention Multimodal Video Forgery Detection

Hoda Osama Elkhodary¹, Sherin Mostafa Youssef¹, Marwa Elshenawy¹, and Dalia Sobhy¹

¹Computer Engineering Department, College of Engineering and Technology, Arab Academy for Science, Technology and Maritime Transport, Alexandria, Egypt, {hudaoelkhodary, sherin, marwa_elshenawy, dalia.sobhi}@aast.edu

Abstract

The rapid advancement of Deepfake technologies and video manipulation tools poses a critical challenge to multimedia forensics, judicial evidence integrity, and information authenticity. Current detectors rely on single-modality signals, treating appearance, geometry, and motion independently. However, advanced generators maintain within-modality consistency while producing cross-modal contradictions, which are forensically discriminative but invisible to any single-modal detector. We propose CAM-VFD, a Cross-Attention Multimodal Video Forgery Detection framework that models cross-modal contradiction as a directional forensic signal. The framework uses a cross-attention fusion mechanism in which CLIP-based appearance representations serve as queries against VideoMAE motion features and MiDaS depth features, enabling the identification of contradictions between visual, temporal, and geometric evidence. We examine this design through cross-modal attention discrepancy analysis, observing statistically separable real and fake distributions ($p < 0.001$, Cohen's $d = 0.68$). Experimental results on two generative video benchmarks indicate consistent performance, with 95.31% Top-1 accuracy on GenVidBench and 93.43% accuracy, 90.63% F1-score, and 96.56% AUROC on GenVideo. Moreover, CAM-VFD demonstrates stable performance under compression, noise, blur, and adversarial perturbations, suggesting that cross-modal reasoning may improve robustness in media forensics. The code is publicly available at <https://github.com/Hoda-Osama/CAM-VFD/tree/main>.

Keywords: Deepfake, Forgery Detection, Forensic, AI-generated content detection, Video Forensics, content authenticity detection, Multimodal Fusion, CLIP, VideoMAE, MiDaS, Cross-Attention Fusion, cross-modal contradiction.

1 Introduction

Recent evolution in artificial intelligence, particularly deep learning-based techniques such as Generative Adversarial Networks (GANs), diffusion models, and auto-regressive architectures, has enabled AI-based synthetic video generators to emerge. Deepfakes—realistic yet fabricated synthetic videos—are becoming increasingly difficult to distinguish with the human eye, challenging the validity of digital media in courts [1]. The consequences are severe: fabricated videos have appeared as forensic evidence in legal proceedings, been exploited to spread political disinformation, and used to impersonate individuals without consent [2]. Consequently, there is an urgent need for reliable and scalable methods for Deepfake detection.

Previous work in video forensics has progressed from detecting spatial artifacts in individual frames [3, 4] to capturing temporal inconsistencies in facial dynamics [5–7]. More recent approaches have explored spatio-temporal feature learning [8, 9] and semantic coherence analysis [10, 11]. However, these approaches fail to generalize to the next-generation generators, which can now synthesize entire semantically rich scenes rather than modifying facial regions using generative models of text-to-video (T2V) [12] or image-to-video (I2V) [13]. Although some recent approaches designed for full-frame manipulations have been developed [14], a fundamental limitation persists in nearly all of them: they treat the video as a collection of signals from a single modality dimension, overlooking cross-modal contradictions and misalignment between appearance, geometry, and motion. These cross-modal contradictions cause a detection failure in current-generation AI video detection models because most AI-generated videos may appear locally plausible in any single modality while containing cross-modal contradictions rarely found in physically captured authentic footage. Although multimodal detection technologies are introduced in some recent works [15, 16], they are still incapable of combining appearance, depth, and motion cues through effective fusion mechanisms. Specifically, most existing multimodal frameworks are not designed to explicitly detect cross-modal contradiction as a forensic signal; they seek to benefit from complementary information without querying one modality for evidence that contradicts another.

In response to these challenges, we propose **CAM-VFD** (Cross-Attention Multimodal Video Forgery Detection), which treats cross-modal contradiction as an explicit, *directional* forensic signal. Appearance is the richest semantic forensic channel as it integrates semantic content, texture, illumination, and object identity, so appearance tokens serve as a forensic query channel while motion and depth provide the key evidence against which appearance is tested. The model computes, for each appearance token, the degree to which the motion and depth context are consistent with that appearance.

Our proposed framework provides the following contributions:

- We introduce **cross-modal contradiction** as a directional forensic signal for Deepfake detection, and validate its forensic separability via attention discrepancy analysis. The results demonstrate a clear and consistent separation between real and fake samples.
- We propose a **cross-attention fusion module** in which CLIP [17] appearance rep-

Table 1: Summary of existing literature.

Ref.	Target Content	Modalities	Fusion Strategy
[8, 9, 21, 22]	Face	Single (Spatio-Temp.)	None
[23, 24]	Face	Single (Spatio-Temp.)	None
[5, 10, 11, 25, 26]	Face	Single (Semantic/Motion)	None
[15, 27, 28]	Face	Two	Simple/Static
[29–31]	Face/Scene	Two–Three	Advanced/Static
Ours	Scene	Three	Cross-attention

representations serve as queries against VideoMAE [18] motion and MiDaS [19, 20] depth as keys and values, operationalizing the directional forensic relationship.

- We conduct a **comprehensive evaluation on two benchmarks** to prove the efficacy of our proposed framework for fake video detection compared to state-of-the-art methods. We tested the model across GenVidBench and GenVideo, achieving higher accuracy compared to the state-of-the-art.
- We perform **robustness and security analysis** under real-world conditions, including compression, noise, blurring, and adversarial perturbations, with direct SOTA comparison against DeMamba under identical settings. The findings suggest improved robustness to challenging degradations while preserving reliable detection performance.

The remainder of this paper is structured as follows. Section 2 discusses the related work. Section 3 describes the proposed CAM-VFD framework. Section 4 presents the experimental results and ablation studies. Section 5 presents the cross-modal attention discrepancy analysis validating our forensic premise. Section 6 reports robustness and adversarial evaluation. Section 7 concludes the paper.

2 Related Work

In this section, we provide a discussion related to major research directions for detecting synthetic videos: (i) *spatio-temporal inconsistencies* (Section 2.1), which focus on defects across space and time; (ii) *semantic and dynamic inconsistency* (Section 2.2), which captures unnatural human motion, action dynamics, or semantic mismatches; and (iii) *multimodal fusion* (Section 2.3), which integrates complementary cues across modalities to expose manipulation traces. Table 1 summarizes the landscape and positions CAM-VFD relative to prior work.

2.1 Spatio-Temporal Inconsistencies

Early detection methods analyzed video frames individually, exploiting trace patterns left by generators in convolutional feature maps [3, 4] or frequency-domain statistics. Research then shifted to spatio-temporal inconsistencies, motivated by the observation that temporal consistency is difficult for generative models to maintain. For instance, early work by [8]

used a 3D convolutional neural network (CNN) on stacked face regions from consecutive frames to capture unnatural transitions. Similarly, [9] proposed a spatio-temporal CNN that analyzes both RGB spatial features and temporal dynamics from optical flow maps. [21] combined three ResNet-50 models targeting spatial, temporal, and structural anomalies with fuzzy logic to handle uncertainty. [22] targeted inter-frame illumination inconsistencies by proposing a learnable Illumination Decomposition Module (IDM) that separates frames into illumination and reflection components. Recently, [23] proposed a dynamic data augmentation strategy guided by forgery heatmaps produced by a Swin Transformer, combined with Cross-Frame Multi-Head Attention (CMA) and a Bidirectional GRU to model sequential spatio-temporal dependencies. To improve generalisation to unseen generation methods, [24] proposed FakeSTormer, a multi-task learning framework with two auxiliary branches targeting spatial and temporal regions independently, paired with a video synthesis strategy redefining Deepfake detection as a fine-grained regression task rather than a binary classification problem. Despite these advances, spatio-temporal methods are insufficient against generators that produce realistic frame-to-frame consistency while introducing cross-modal contradictions invisible to within-modality analysis.

2.2 Semantic and Dynamic Inconsistency

AI-generated videos often fail to replicate natural biomechanics and logical scene coherence; the scene as a whole does not appear reasonable and contextually continuous, so recent approaches have begun to explore human motion and semantic forensics. For example, [5] demonstrated the importance of facial features in this context—Deepfakes often violate natural head motion constraints. [10] utilized CLIP embeddings to find semantic mismatches between expected human behavior and generated motion patterns. Other methods proposed in [25] detected unnatural temporal flicker in synthetic movements using frequency-domain motion representations. [26] proposed a cross-branch fusion to analyze dynamic inconsistencies in facial movements. [11] focused on local motion patterns between adjacent frames, which are often overlooked by temporal models. These methods demonstrate that dynamic cues carry forensic information, yet they operate within a single temporal or semantic dimension without grounding evidence in geometric or appearance context.

2.3 Multimodal Fusion

Integrating multiple modality streams has become a direction for recent research work, motivated by the complementary forensic evidence that different modalities provide. [15] introduced M2TR, a multimodal transformer model fusing visual and spectral cues through a cross-modality fusion block. [27] developed AVFF, a two-stage multimodal approach that learns cross-modal audio-visual correspondences through self-supervised pre-training. [28] proposed an Ensemble of Experts model that synthesizes three modalities: appearance, motion, and geometry. More recent works have substantially advanced the sophistication of multimodal fusion strategies. [29] proposed CAD (Cross-Modal Alignment and Distillation), a dual-path architecture combining a cross-modal component that catches semantic mismatches and a distillation mechanism that preserves important modality-specific features. [30] used an attention mechanism to fuse local spatial features with global frequency-

domain statistics, demonstrating the importance of inter-modal relationships. [31] proposed a multimodal Deepfake detection framework that models cross-modal consistency between facial dynamics and scene context, demonstrating the forensic signals in cross-modal inconsistency. The critical limitation shared by these methods is their use of symmetric or static fusion—a fixed aggregation of modality features—regardless of which forensic signal is most informative for a given input. In CAM-VFD, by contrast, appearance serves as the forensic query channel: the model asks, for each appearance token, whether the motion and depth evidence support or contradict it.

3 The Proposed CAM-VFD

In this section, we first present the overall framework of CAM-VFD, then describe each module in detail: adaptive frame sampling, modality-specific feature extraction, cross-modal attention fusion, and the classification layer.

3.1 Overview

The proposed CAM-VFD framework, illustrated in Figure 1, uses three modality-specific encoders and a cross-attention fusion module operating in a unified latent space. Given a video $\mathbf{V} = \{x_1, \dots, x_T\}$, the framework outputs a binary prediction $\hat{y} \in \{\text{Real}, \text{Fake}\}$.

The processing pipeline proceeds as follows. Frames are first adaptively sampled to T and augmented during training. Three pre-trained encoders then extract modality-specific features independently: CLIP [17] for appearance, MiDaS [19, 20] DPT-Hybrid for depth, and VideoMAE [18] for motion. All features are projected into a shared dimensional space. Appearance features are temporally encoded by a Transformer encoder; they then serve as queries in two parallel cross-attention blocks, one against *motion* features and one against *depth* features. The three pooled feature streams are concatenated and classified by an MLP. Algorithm 1 summarizes the complete pipeline.

3.2 Adaptive Frame Sampling

Fake videos vary substantially in length and frame rate (*fps*), which can disrupt feature consistency and forensic traces. Fixed-interval sampling may miss key artifact locations, and we need the most temporal coverage with motion cues of the videos; therefore, we use an *adaptive consecutive* frame sampling technique motivated by the principle that adaptive selection improves temporal coverage and efficiency [32]. We select T frames using a video-length-dependent policy: for *short* videos with fewer frames than T , we use cyclic repetition to preserve motion continuity. For *medium-length* videos containing nT frames, we select consecutive frame segments from different regions—from the beginning and end—to capture both local motion smoothness and global temporal variation. For *long* videos with more than nT frames, we extract distributed segments from the beginning, middle, and end to provide broader temporal coverage. This adaptive segmentation enables the model to detect temporal irregularities and motion inconsistencies that are characteristic of manipulated content.

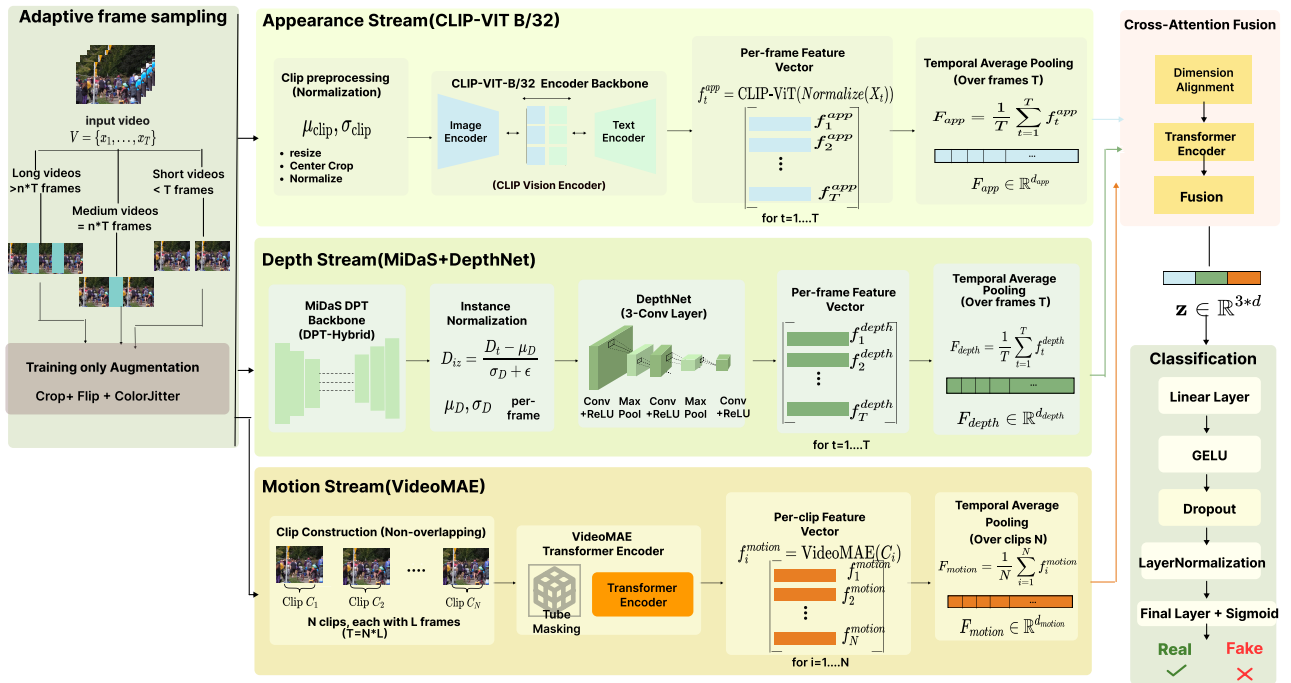


Figure 1: Proposed Cross-Attention Multimodal Video Forgery Detection (CAM-VFD) Framework.

Deep models tend to memorize pixel patterns, lighting, and other artifacts from the training data; thus, during training only, frames are augmented with `RandomResizedCrop` and `Flip` to simulate different viewing conditions such as different zoom levels and camera framing, and `ColorJitter` to enhance the model’s resilience to changes in lighting and color [33].

3.3 Modality-Specific Feature Extraction

Despite the significant advancements in AI video generators, they fail to produce fake videos that are indistinguishable from real ones. In some cases, each appearance, motion, and depth representation may appear independently plausible, while there is a contradiction between how a scene looks, how it moves, and how it is geometrically structured. As illustrated in Figure 2, real videos exhibit high internal consistency across appearance, depth, and motion, whereas fake videos expose distinctive inconsistency signatures across all three modalities. Three pre-trained backbones extract modality-specific forensic cues independently prior to fusion, allowing for a comprehensive analysis of the inconsistencies present in the appearance, motion, and depth representations of the videos.

3.3.1 Appearance Features

Manipulated videos often contain visual attributes detectable by deep models but not by the human eye. Common types include: (i) **Texture Abnormalities:** unnatural skin texture, over-smoothed textures, and inconsistent reflections and shadows; (ii) **Boundary**

Algorithm 1 CAM-VFD: Cross-Attention Multimodal Video Forgery Detection

INPUT: Video $V = \{x_1, \dots, x_T\}$
OUTPUT: $y \in \{\text{Real}, \text{Fake}\}$
1. Preprocessing: Adaptive frame sampling + augmentations
2. Appearance Features:
for each frame x_t do
 $f_t^{\text{app}} = \text{CLIP-ViT}\left(\frac{x_t - \mu_{\text{clip}}}{\sigma_{\text{clip}}}\right)$
end for
 $F_{\text{app}} = \frac{1}{T} \sum_t f_t^{\text{app}}$
3. Depth Features:
for each frame x_t do
 $D_t = \text{MiDaS}(x_t)$; $f_t^{\text{depth}} = \text{DepthNet}(\text{BN}(\frac{D_t - \mu_D}{\sigma_D + \epsilon}))$
end for
 $F_{\text{depth}} = \frac{1}{T} \sum_t f_t^{\text{depth}}$
4. Motion Features:
for each clip C_c do
 $f_i^{\text{motion}} = \text{VideoMAE}(C_i)$
end for
 $F_{\text{motion}} = \frac{1}{N} \sum_{i=1}^N f_i^{\text{motion}}$
5. Fusion & Classification:
 $H_{\text{app}} = W_{\text{app}} F_{\text{app}}$, $H_{\text{depth}} = W_{\text{depth}} F_{\text{depth}}$, $H_{\text{motion}} = W_{\text{motion}} F_{\text{motion}}$
 $H_{\text{app}}^{\text{temp}} = \text{TransformerEncoder}(H_{\text{app}} + PE)$
 $H_{\text{app-motion}} = \text{Attn}(H_{\text{app}}^{\text{temp}}, H_{\text{motion}})$, $H_{\text{app-depth}} = \text{Attn}(H_{\text{app}}^{\text{temp}}, H_{\text{depth}})$
 $z = [\frac{1}{T} \sum H_{\text{app}}^{\text{temp}}; \frac{1}{T} \sum H_{\text{app-motion}}; \frac{1}{T} \sum H_{\text{app-depth}}]$
 $p = \sigma(\text{MLP}(z))$
 $y = \text{Real if } p \geq 0.5 \text{ else Fake}$
return y

Artifacts: distorted edges, misaligned facial features, and loss of fine structural details;
(iii) Inconsistent Illumination: color mismatches, unnatural gradients, and spatially inconsistent lighting.

We extract appearance features using the Vision Transformer (ViT-B/32) variant of the CLIP (Contrastive Language–Image Pre-training) model [17]. CLIP is a recent vision-language model which captures rich semantic and structural attributes including facial anatomy, texture realism, and geometric alignment. As shown in Figure 2 (row 2), real video shows coherent and consistent attention patterns across all sampled frames. In contrast, fake video shows fragmented attention maps, indicating texture and appearance inconsistencies.

Each input video frame X_t is first resized and normalized using CLIP-specific parameters (μ_{clip} , σ_{clip}). Then the appearance feature vector f_t^{app} for each processed frame is extracted by the CLIP Vision Transformer encoder:

$$f_t^{\text{app}} = \text{CLIP-ViT}\left(\frac{X_t - \mu_{\text{clip}}}{\sigma_{\text{clip}}}\right) \quad (1)$$

To obtain the appearance representation F_{app} , we use temporal average pooling (where d_{app}

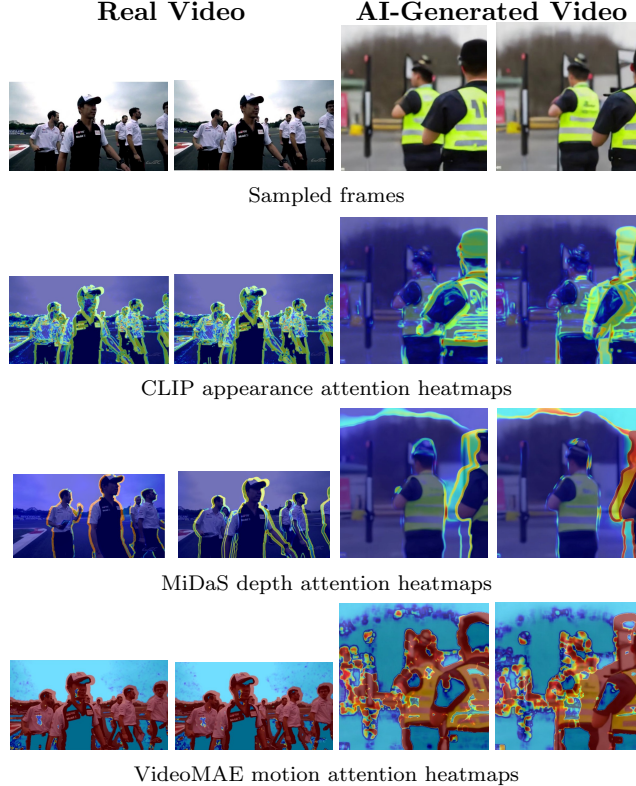


Figure 2: **Multimodal feature heatmaps extracted from real and AI-generated video samples by CAM-VFD.** Across all three modalities, real videos (left) exhibit strong cross-modal consistency, with coherent spatial structures, stable depth transitions, and physically plausible motion patterns reflecting underlying scene geometry. In contrast, AI-generated videos (right) expose distinctive inconsistency signatures: fragmented and spatially unstable appearance activations, geometrically incoherent depth transitions at subject boundaries, and abnormal motion energy concentrations at biologically unrealistic locations.

is the dimensionality of the appearance feature vector):

$$F_{app} = \frac{1}{T} \sum_{t=1}^T f_t^{app} \in \mathbb{R}^{d_{app}} \quad (2)$$

3.3.2 Depth Features

Depth features capture the 3D geometric structure of objects and scenes. Real videos exhibit consistent depth, whereas AI-generated videos often contain: **(i) Geometric Structure Inconsistency:** distorted or unrealistic depth patterns; **(ii) Flattened or Collapsed Depth:** inconsistent or flattened geometric structures, such as unrealistic facial depth; and **(iii) Depth Discontinuities at Object Boundaries:** distorted background due to imperfect 3D rendering. To capture the underlying 3D geometry and spatial consistency within each frame, we use the MiDaS (Monocular Depth Estimation in the Wild) DPT-Hybrid

model [19] for computing per-frame depth maps. MiDaS is robust to color variations, illumination changes, and scene diversity. As shown in Figure 2 (row 3), real videos exhibit smooth and spatially consistent depth distributions across both foreground subjects and background regions, indicating coherent 3D scene geometry. In contrast, fake videos expose geometric inconsistencies and unnatural spatial relationships between the two subjects and the background.

The extraction of depth maps for each frame is performed as follows, where D_t represents the raw depth map for input frame X_t with a resolution of $H \times W$ pixels:

$$D_t = \text{MiDaS}(X_t) \in \mathbb{R}^{H \times W} \quad (3)$$

Then the depth maps for each input frame are normalized:

$$D_{iz} = \frac{D_t - \mu_D}{\sigma_D + \epsilon} \quad (4)$$

where D_{iz} is the instance-normalized depth map. Subsequently, to eliminate the effect of global lighting, the normalized depth maps D_{iz} are processed using a lightweight CNN-based encoder (DepthNet: 3 convolutional layers, max-pool, 128-d output) with batch normalization to obtain depth embeddings:

$$f_t^{depth} = \text{DepthNet}(\text{BN}(D_{iz})) \quad (5)$$

Here, BN denotes Batch Normalization. Finally, the depth representation is obtained by averaging across all sampled frames (where d_{depth} is the dimensionality of the depth feature vector):

$$F_{depth} = \frac{1}{T} \sum_{t=1}^T f_t^{depth} \in \mathbb{R}^{d_{depth}} \quad (6)$$

3.3.3 Motion Features

Motion features capture temporal inconsistencies in pixels, objects, or regions in video frames; they detect: **(i) Unsynchronized Motion:** when background and foreground are at mismatched speeds; **(ii) Temporal Flickering:** inconsistent brightness and textures; and **(iii) Physics Violations:** unrealistic movement or collision of objects. We use the VideoMAE (Video Masked Autoencoder) transformer encoder [18] to capture temporal dynamics glitches. VideoMAE is a self-supervised pre-trained model designed for video understanding. As shown in Figure 2 (row 4), real videos exhibit smoothly and consistently distributed motion across moving body parts, indicating stable temporal dynamics. In contrast, fake videos reveal abnormal temporal variation and motion inconsistency.

Given the adaptively sampled sequence of frames, non-overlapping clips C_i are constructed and fed into the model’s dedicated image processor. For each clip, the motion feature vector f_i^{motion} is extracted from the last hidden state of the VideoMAE:

$$f_i^{motion} = \text{VideoMAE}(C_i) \quad (7)$$

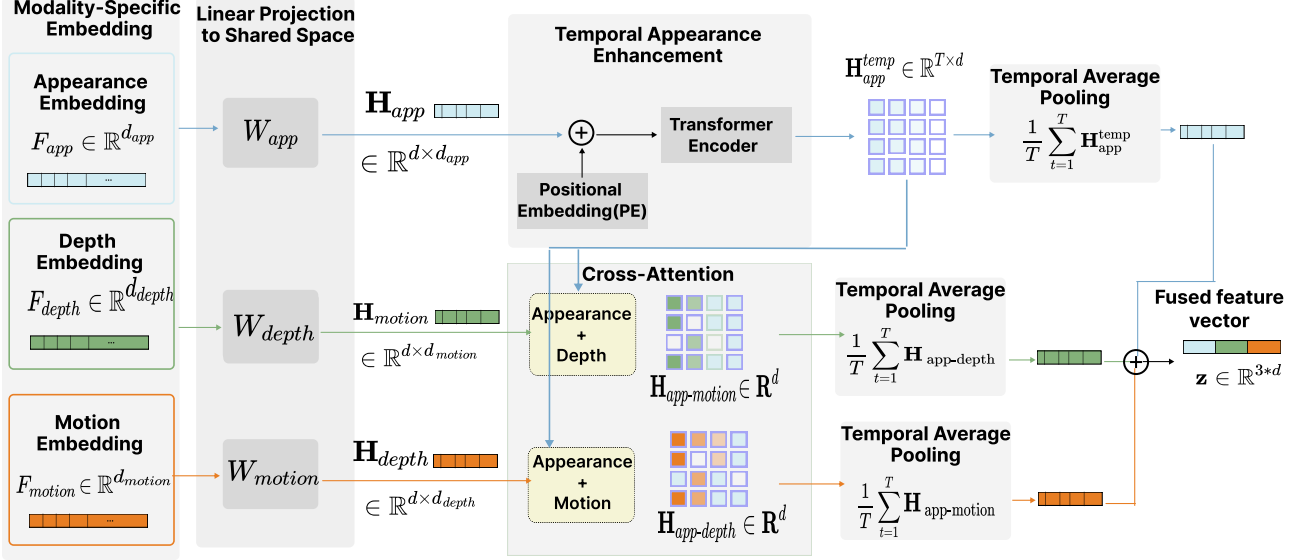


Figure 3: Overview of the proposed cross-attention fusion mechanism.

The global motion embedding F_{motion} is computed as the average across all clips (where d_{motion} is the dimensionality of the motion feature vector):

$$F_{motion} = \frac{1}{N} \sum_{i=1}^N f_i^{motion} \in \mathbb{R}^{d_{motion}} \quad (8)$$

3.4 Cross-Modal Fusion

After extracting the feature representations, it is necessary to combine them for the *classification* stage. A simple concatenation fusion would fail because it computes appearance-to-depth alignment and depth-to-appearance alignment, treating both directions as equally informative, losing the directional forensic structure. However, symmetric cross-attention improves upon concatenation but still lacks directional reasoning.

Our key insight is that CLIP appearance features encode a rich semantic prior regarding the expected appearance of a scene. This integration of semantic content, texture, illumination, and object identity allows appearance to serve as a natural forensic query channel. By leveraging appearance as queries and motion/depth as keys and values, the model explicitly poses the question: *Given the appearance of this scene, do the motion and depth evidence support or contradict it?* Figure 3 provides a more detailed illustration of the fusion architecture.

For appearance (F_{app}), motion (F_{motion}), and depth (F_{depth}) features, we use linear transformations to project them into a shared dimensional space:

$$\mathbf{H}_{app} = \mathbf{W}_{app} \mathbf{F}_{app} \in \mathbb{R}^{d \times d_{app}} \quad (9)$$

$$\mathbf{H}_{motion} = \mathbf{W}_{motion} \mathbf{F}_{motion} \in \mathbb{R}^{d \times d_{motion}} \quad (10)$$

$$\mathbf{H}_{depth} = \mathbf{W}_{depth} \mathbf{F}_{depth} \in \mathbb{R}^{d \times d_{depth}} \quad (11)$$

where $\mathbf{W}_* \in \mathbb{R}^{d \times d_{in}}$ are learnable projection matrices, d represents the shared latent dimensionality, and d_{app} , d_{motion} , and d_{depth} are the input feature dimensionality for the appearance, motion, and depth modalities, respectively. Projecting all modalities into a unified dimensional space ensures consistent feature scaling and allows the cross-attention module to effectively learn inter-modal dependencies.

To capture inter-frame dependencies before cross-modal querying, the sequence of appearance embeddings \mathbf{H}_{app} is passed through a Transformer encoder with learnable positional embedding (PE) to preserve frame order, yielding temporally-enhanced features \mathbf{H}_{app}^{temp} :

$$\mathbf{H}_{app}^{temp} = \text{Transformer}(\mathbf{H}_{app} + \mathbf{PE}) \in \mathbb{R}^{T \times d} \quad (12)$$

where T denotes the number of sampled frames and d represents the shared latent dimensionality of the temporal transformer encoder. To enable dynamic, content-aware fusion of multimodal features, we developed two parallel cross-attention mechanisms. The *first* mechanism computes interactions between appearance and motion features to identify discrepancies between an object’s visual representation and its movement. The *second* mechanism evaluates interactions between appearance and depth features to locate areas where the shape of the object does not correspond with its visual texture. The computation for the appearance-motion interaction is formalized in Equation 13, where the temporally enhanced appearance features act as the Query ($Q_{app} = H_{app}^{temp}$), while the motion features serve as both the Key and Value ($K_{motion} = V_{motion} = H_{motion}$). In a parallel approach, using H_{depth} for the Key and Value calculates the appearance-depth interaction features $H_{app-depth}$, as shown in Equation 14.

$$\mathbf{H}_{app-motion} = \text{softmax}\left(\frac{\mathbf{Q}_{app}\mathbf{K}_{motion}^\top}{\sqrt{d}}\right)\mathbf{V}_{motion} \quad (13)$$

$$\mathbf{H}_{app-depth} = \text{softmax}\left(\frac{\mathbf{Q}_{app}\mathbf{K}_{depth}^\top}{\sqrt{d}}\right)\mathbf{V}_{depth} \quad (14)$$

This design means each appearance token explicitly attends to the motion and depth context: *low* attention weights indicate consistent evidence; anomalously *high* or structured weights indicate forensic contradiction. The outputs from each cross-attention block $H_{app-motion}$, $H_{app-depth}$, and the temporal appearance features H_{app}^{temp} are pooled by averaging over T (the number of sampled frames per video) and concatenated to form a unified video representation z :

$$z = \left[\frac{1}{T} \sum_{t=1}^T H_{app}^{temp}; \frac{1}{T} \sum_{t=1}^T H_{app-motion}; \frac{1}{T} \sum_{t=1}^T H_{app-depth} \right] \in \mathbb{R}^{3d} \quad (15)$$

3.5 Classification Layer

The fused representation z is processed through a multi-layer perceptron (MLP) classifier with two hidden layers; each layer incorporates GELU activation functions to introduce non-linearity, followed by dropout for regularization and layer normalization. A final linear layer

with a sigmoid activation function outputs a binary prediction score between 0 and 1. We classify the video as *Real* if $p \geq 0.5$ and *Fake* otherwise. The complete prediction pipeline, termed CAM-VFD, is formally defined as:

$$p = \text{CAM-VFD}(\mathbf{V}) = \text{MLP}(z) \in [0, 1] \quad (16)$$

4 Experiments

This section describes the comprehensive evaluation of CAM-VFD. First, we introduce the experimental settings. Next, we present the performance of our model against two benchmark datasets. Then, we conduct ablation studies to analyze the contribution of different components. Finally, we perform robustness tests to measure how well our model performs under varying perturbations.

4.1 Experimental Settings

4.1.1 Datasets

We evaluate CAM-VFD on two complementary benchmarks: GenVidBench [34] and GenVideo [35]. Together, they provide complementary generalisation evidence: source-aligned cross-generator robustness vs. zero-shot transfer to maximally diverse unseen scenarios.

GenVidBench [34] is a challenging benchmark for AI-generated video detection, which addresses real-world generalization, semantic diversity, and cross-generator robustness. It contains 143,400 videos of multiple resolutions, durations, and generative methods, including 33,931 real videos and 109,200 synthetic videos generated by eight state-of-the-art diffusion-based and auto-regressive models using Text-to-Video (T2V) [12] and Image-to-Video (I2V) [13] frameworks. It is source-aligned: each synthetic video is generated from the same text prompt or source image as its paired real video, increasing the difficulty of the detection task and forcing detectors to rely on subtle forensic artifacts rather than dataset biases.

GenVideo [35] is a million-scale AI-generated video detection benchmark comprising over 1,078,838 generated videos and 1,223,511 real videos. Synthetic videos span 20 distinct state-of-the-art generators and real videos span 3 diverse sources. The scale and diversity of GenVideo prevent content-level shortcut exploitation, instead compelling identification of subtle modality-level authenticity cues.

4.1.2 Implementation Details

We fix the temporal dimension to $T = 16$ sampled frames employing the adaptive consecutive sampling strategy, which adjusts the sampling technique according to the length of the input video, selecting (6, 5, 5) frames for *long* videos, two 8-frame segments for *medium-length* videos, and cyclic repetition for *short* clips. During input preprocessing, video frames are resized to 256×256 and randomly cropped to 224×224 ; the training set is augmented using

`RandomResizedCrop` (scale $[0.8, 1.0]$), horizontal flipping ($p = 0.5$), and `ColorJitter` with brightness 0.2, contrast 0.2, saturation 0.1, and hue 0.1.

For feature extraction, CLIP ViT-B/32 is used for appearance, VideoMAE-Base for motion, and MiDaS DPT-Hybrid for depth estimation, each producing 512, 768, and 128 dimensional feature vectors, respectively. All modality features are projected into a unified 256-dimensional space. The cross-attention fusion employs two multi-head attention blocks (8 heads, $d = 256$). The final classifier consists of linear layers of sizes 768, 512, 256, 1, using GELU activations, LayerNorm, and dropout rates of 0.5 and 0.3.

All experiments use the Adam optimiser with a learning rate of 1×10^{-5} and cosine annealing schedule, trained for 50 epochs with early stopping (patience = 10) on a held-out 10% validation split and batch size 32. The three pre-trained backbones are frozen during training; only the projection layers, transformer encoder, cross-attention modules, and MLP classifier are optimised.

4.1.3 Evaluation Metrics

On GenVidBench, we report per-generator accuracy and Top-Mean Accuracy following the standard evaluation protocol [34]. On GenVideo, we report Recall, Accuracy, F1-score, and AUROC per generation scenario and overall average, following the standard evaluation protocol [35].

4.2 Results

4.2.1 Comparison on GenVidBench

Table 2 presents a comparative evaluation of our model against state-of-the-art CNN-based and Transformer-based video classification models. Training uses videos from Pika, VC2, ModelScope, and Text2Video-Zero (Group 1) and Vript real videos. Testing uses unseen generators from Group 2 (MuseV, SVD, CogVideo, Mora) and HD-VG-130M. This challenging setup forces the model to generalize to unseen generation sources. No single-stream baseline achieves above 83% mean accuracy, while CAM-VFD exceeds 90% on all five subsets, demonstrating strong robustness to unseen generation methods.

CAM-VFD achieves 95.31% mean Top-1 accuracy, outperforming the best baseline (MViT V2, 83.27%) by 12.04%, while maintaining above 90% accuracy on every subset. Accuracy reaches 99.74% on CogVideo and 99.52% on HD-VG. Traditional CNN and Transformer models struggle with generalization as they rely mainly on appearance cues—for example, MViT V2 achieves 98.29% on SVD but only 47.50% on CogVideo. In contrast, CAM-VFD leverages cross-modal contradiction to capture spatial, temporal, and geometric inconsistencies, supported by a cross-attention fusion mechanism that enhances robustness across all tested generators.

Table 2: Comparison with state-of-the-art baselines on GenVidBench. Models are trained on Pika, VC2, ModelScope, Text2Video-Zero and Vript; tested on unseen sources HD-VG-130M, CogVideo, SVD, MuseV, and Mora. Best result in **bold**.

Model	Type	HD-VG	CogVideo	SVD	MuseV	Mora	Mean
I3D [36]	CNN	93.99	60.11	8.29	8.15	59.24	45.96
SlowFast [37]	CNN	93.63	38.34	12.68	12.25	45.93	40.57
TPN [38]	CNN	97.34	68.25	8.79	37.86	90.04	60.46
TIN [39]	CNN	97.88	81.59	21.47	33.78	79.44	62.83
X3D [40]	CNN	97.51	65.72	37.27	92.39	49.60	68.50
TRN [41]	CNN	93.97	91.34	26.64	38.92	93.98	68.97
TSM [42]	CNN	96.76	78.46	54.70	70.37	70.37	74.13
UniFormerV2 [43]	Xfmr	96.89	45.21	14.81	20.05	99.21	55.23
TimeSformer [44]	Xfmr	92.32	74.80	20.17	73.14	39.40	59.97
VideoSwin [45]	Xfmr	98.55	88.47	68.48	49.11	81.42	77.21
MViT V2 [46]	Xfmr	97.58	47.50	98.29	76.34	96.62	83.27
CAM-VFD (ours)	Multi.	99.52	99.74	92.85	92.10	92.36	95.31

Xfmr: Transformer. Multi.: Multimodal.

4.2.2 Comparison on GenVideo

We evaluate CAM-VFD on the GenVideo benchmark [35] to validate its generalization beyond the GenVidBench setting. Models are trained on 10,000 real videos from Kinetics-400 and 10,000 generated videos from Pika, then evaluated on ten generation scenarios entirely unseen during training. Table 3 reports Recall, Accuracy, F1-score, and AUROC across all scenarios and compares CAM-VFD against four competitive baselines.

CAM-VFD achieves 93.43% average Accuracy (+9.22% over DeMamba [35], +2.19% over NSG-VD [47]) and 96.56% AUROC, maintaining high performance across all ten unseen scenarios. In contrast, prior methods suffer from severe per-generator degradation; for instance, STIL [48] collapses to 1.40% recall on HotShot and 2.00% on Show1, while NPR [49] drops to 16.00% and 33.00% respectively. CAM-VFD’s worst-case recall drops to 82.30% on Moon Valley, which contains near-static scenes with minimal foreground motion that reduces the discriminability of VideoMAE features. These results confirm that CAM-VFD’s cross-modal contradiction architecture captures fundamental forensic signals, enabling strong zero-shot generalization.

4.3 Generalization Evaluation

To examine our method’s generalizability, Table 4 reports performance under In-Distribution (ID) and Out-of-Distribution (OOD) evaluation on GenVidBench. ID means testing on the same generator seen during training; OOD means testing on a different unseen generator. In

Table 3: Comparison with state-of-the-art baselines on GenVideo. Models trained on 10K real (Kinetics-400) and 10K generated (Pika); evaluated on unseen generators. Best results in **bold**.

Method	Metric	Morph Studio	Model Scope	Moon Valley	Hot-Shot	Show1	Gen2	Craft	LaVie	Sora	Wild Scrape	Avg.
DeMamba [35]	Recall	87.00	93.60	98.80	40.60	48.40	98.00	88.40	59.00	48.21	58.20	72.02
	Accuracy	91.70	95.00	97.60	68.50	72.40	97.20	92.40	77.70	72.32	77.30	84.21
	F1	91.29	94.93	97.63	56.31	63.68	97.22	92.08	72.57	63.53	71.94	80.12
	AUROC	98.04	98.82	99.68	87.84	90.12	99.46	97.81	91.32	88.36	87.38	93.88
NPR [49]	Recall	61.20	80.00	98.00	16.00	33.00	91.20	80.60	34.60	35.71	43.20	57.35
	Accuracy	79.80	89.20	98.20	57.20	65.70	94.80	89.50	66.50	67.86	70.80	77.96
	F1	75.18	88.11	98.20	27.21	49.03	94.61	88.47	50.81	52.63	59.67	68.39
	AUROC	93.05	97.18	99.66	82.97	90.50	99.13	97.87	87.54	90.47	91.84	93.02
TALL [50]	Recall	51.20	65.20	93.40	32.00	61.60	94.80	81.80	49.20	25.00	53.60	60.78
	Accuracy	75.10	82.10	96.20	65.50	80.30	96.90	90.40	74.10	61.61	76.30	79.85
	F1	67.28	78.46	96.09	48.12	75.77	96.83	89.50	65.51	39.44	69.34	72.63
	AUROC	95.82	97.14	99.73	92.55	97.36	99.79	99.09	94.84	86.67	93.75	95.67
STIL [48]	Recall	73.80	70.80	43.40	1.40	2.00	45.00	13.20	7.20	1.79	11.60	27.02
	Accuracy	86.90	85.40	71.70	50.70	51.00	72.50	56.60	53.60	50.89	55.80	63.51
	F1	84.93	82.90	60.53	2.76	3.92	62.07	23.32	13.43	3.51	20.79	35.82
	AUROC	96.43	97.77	99.34	86.66	90.56	98.88	97.04	88.16	92.57	87.52	93.49
NSG-VD [47]	Recall	68.33	98.33	100.00	92.50	87.50	80.00	98.33	94.17	78.57	82.50	88.02
	Accuracy	81.67	98.33	96.67	91.67	90.83	88.33	95.83	94.17	88.39	88.75	91.46
	F1	78.85	98.33	96.77	91.74	90.52	87.27	95.93	94.17	87.13	88.00	90.87
	AUROC	92.26	98.66	98.15	94.45	96.38	94.83	98.16	97.41	96.40	94.73	96.14
CAM-VFD (ours)	Recall	85.20	89.50	82.30	91.80	90.50	86.70	93.20	88.40	83.60	87.90	87.91
	Accuracy	92.50	94.80	90.60	95.90	95.10	93.20	96.80	93.60	89.50	92.30	93.43
	F1	88.70	92.10	86.40	93.80	92.80	89.90	95.00	91.00	86.50	90.10	90.63
	AUROC	95.80	97.20	94.90	98.10	97.60	96.40	98.70	96.90	93.80	96.20	96.56

Group 1 (Pika, VideoCrafter2, ModelScope, and Text2Video-Zero), all videos share identical text prompts. In Group 2, videos are generated from either the same image (MuseV, SVD) or the same text prompt (CogVideo, Mora).

The ID-to-OOD accuracy drop for CAM-VFD is minimal: from 99.20% to 97.52% for Group 1 (mean drop of 1.68%) and from 96.61% to 93.98% for Group 2 (mean drop of 2.63%). By comparison, VideoSwin-Tiny achieves only 56.71% OOD on Group 2 under equivalent conditions [34]. These results highlight that cross-modal contradiction is a generator-agnostic forensic signal that does not overfit to the artifact characteristics of any specific generation method.

4.4 Ablation Study

All ablation studies isolate one component while holding the others fixed, compared to the full model (three modalities, 16 frames, cross-attention fusion) trained and tested on ModelScope and Vript, achieving 99.91% accuracy.

4.4.1 Modality Ablation

Table 5 shows an accuracy comparison between the full model and multiple modality configurations, proving the impact of different input modalities. *Appearance-only* achieves 86.0%, confirming that visual semantics provides a useful baseline. However, *motion* features achieve

Table 4: Cross-generator generalization performance across in-distribution (ID) and out-of-distribution (OOD) generators.

Video Source	ID Acc. (%)	OOD Acc. (%)
<i>Group 1: Text-to-Video Generators</i>		
Pika	98.02	97.37
VideoCrafter2	99.31	98.05
Text2Video-Zero	99.55	95.66
ModelScope	99.91	99.00
Mean	99.20	97.52
<i>Group 2: Image/Text-to-Video & High-Quality Fakes</i>		
SVD	92.97	89.71
MuseV	95.94	92.15
Mora	97.63	94.27
CogVideo	99.89	99.80
Mean	96.61	93.98

93.0%, highlighting that temporal dynamics are more discriminative than static appearance. *Depth*-only achieves 82.0%, showing that geometric cues are most valuable in combination. The combination of modalities improves accuracy substantially: appearance and motion reaches 98.0%, appearance and depth reaches 97.0%, and motion and depth achieves 95.0%. The full three-modality model with cross-attention fusion achieves 99.91%, confirming that each modality provides complementary forensic evidence.

4.4.2 Temporal Ablation

Table 6 explores the effects of varying the number of input frames, fixing the model to use all modalities and attention fusion. Using only 8 frames achieves an accuracy of 90%, indicating insufficient temporal coverage. Increasing to 16 frames improves accuracy to 99.91%. A 32-frame configuration reaches 99.95%, confirming that a longer temporal window allows the model to learn more discriminative features. However, the marginal gain from 16 to 32 frames is only +0.04%, revealing that doubling the number of frames yields only a minimal gain in accuracy at double the computational cost. Therefore, 16 frames are selected as the optimal temporal balance.

4.4.3 Fusion Strategy and Query Direction Ablation

Table 7 evaluates various architectural strategies for cross-modal integration and validates the asymmetric design direction. Simple concatenation achieves 90%, confirming that naive feature stacking fails to capture inter-modal dependencies. Late fusion, which aggregates predictions after each stream, improves results to 97.5%. Symmetric cross-attention further improves accuracy to 98.40%, demonstrating the importance of feature interaction but high-

Table 5: Modality contribution ablation.

Configuration	Acc. (%)
Appearance only	86.00
Motion only	93.00
Depth only	82.00
Appearance + Motion	98.00
Appearance + Depth	97.00
Motion + Depth	95.00
All modalities (proposed)	99.91

Table 6: Temporal window ablation.

Frame Count	Acc. (%)
8 frames	90.00
16 frames (selected)	99.91
32 frames	99.95

lighting the limitation of treating modalities equivalently without directional structure. To prove that modeling directional relationships is critical, we evaluate motion-as-query and depth-as-query, achieving 97.23% and 96.88% respectively. The proposed cross-attention fusion (appearance as query, motion and depth as keys/values) achieves 99.91%. These results demonstrate that the performance gains of CAM-VFD arise from structured cross-modal reasoning rather than simple multi-stream aggregation.

5 Cross-Modal Attention Discrepancy Analysis

CAM-VFD is grounded in a core forensic insight: real videos are physically consistent across appearance, geometry, and motion, as they arise from the same real-world scene. In contrast, AI-generated videos are produced through pipelines whose components lack this physical consistency constraint, producing cross-modal contradictions that are detectable even when each modality appears individually plausible.

Given a video $V = \{x_1, \dots, x_T\}$, we define the Cross-Modal Attention Discrepancy (CMAD) as:

$$\text{CMAD}(V) = \frac{1}{2T} \sum_{t=1}^T \left(\left\| \mathbf{H}_{\text{app-motion}}^{(t)} - \mathbf{H}_{\text{app}}^{\text{temp},(t)} \right\|_2^2 + \left\| \mathbf{H}_{\text{app-depth}}^{(t)} - \mathbf{H}_{\text{app}}^{\text{temp},(t)} \right\|_2^2 \right) \quad (17)$$

where $\mathbf{H}_{\text{app}}^{\text{temp}}$ is the temporal appearance features and $\mathbf{H}_{\text{app-motion}}$, $\mathbf{H}_{\text{app-depth}}$ are the cross-

Table 7: Fusion strategy and query direction ablation.

Fusion Method	Acc. (%)
Concatenation	90.00
Late fusion	97.50
Symmetric cross-attention	98.40
Motion queries, App. K/V	97.23
Depth queries, App. K/V	96.88
App. queries (proposed)	99.91

Table 8: Cross-Modal Attention Discrepancy (CMAD) statistical analysis on GenVideo.

Statistic	Real Videos	Fake Videos
Sample size (n)	10,000	10,000
Mean CMAD (μ)	0.160	0.242
Std. deviation (σ)	0.115	0.125
<i>Welch two-sample t-test (real vs. fake)</i>		
t -statistic ($df = 19,998$)	48.1	
p -value	< 0.001	
Cohen’s d	0.68	
Pooled SD	0.120	

attended representations after querying motion and depth respectively. CMAD measures the degree of cross-modal inconsistency by quantifying how much the motion and depth evidence contradict the appearance evidence. Under this formulation, real videos are expected to produce low CMAD values, whereas fake videos produce higher CMAD values.

To validate that CMAD separates real from fake videos, we compute CMAD across the GenVideo benchmark. As shown in Figure 4, real videos exhibit consistently low discrepancy values, reflecting coherent cross-modal alignment consistent with physical reality. In contrast, fake videos produce significantly higher and more localized discrepancy patterns corresponding to cross-modal contradictions.

To assess statistical significance, we perform a two-sample t -test on the CMAD distributions of real and fake videos [51] as shown in Table 8. The test yields a highly significant separation $p < 0.001$, confirming that the observed difference is not due to random variation. We further report Cohen’s d as an effect size measure [52], indicating a large effect size ($d = 0.68$) between the two distributions. These results confirm that the cross-modal contradiction signal is strongly discriminative and is consistent with the qualitative feature heatmap visualisations in Figure 2, which visibly demonstrate cross-modal incoherence in fake videos across all three modality branches.

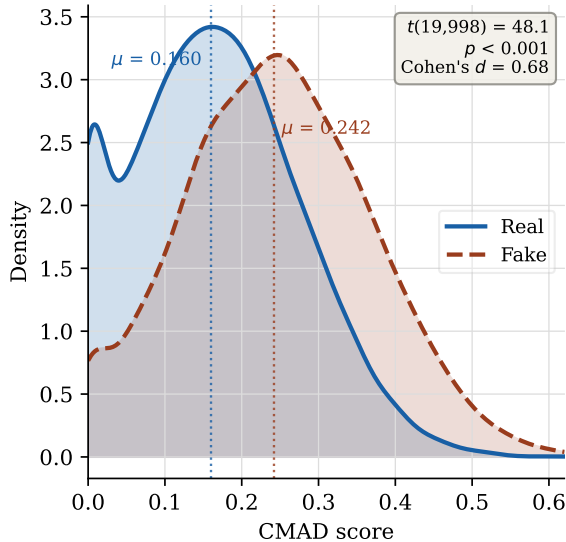


Figure 4: Distribution of Cross-Modal Attention Discrepancy (CMAD) scores for real and fake videos on the GenVideo benchmark.

6 Robustness Evaluation

We evaluated the model’s robustness under real-world conditions across two complementary threat categories: passive signal degradation (Section 6.1) and active adversarial attack (Section 6.2). All experiments are conducted on two representative GenVidBench subsets: CogVideo (highest accuracy, 99.68%) and SVD (lowest accuracy, 90.22%). DeMamba [35] is evaluated under identical corruption conditions throughout Table 9.

6.1 Signal Degradation Robustness

Table 9 presents accuracy under three categories of passive signal degradation: video compression (Constant Rate Factor $CRF \in \{18, 28, 32\}$, where higher CRF indicates heavier compression), additive noise (Gaussian $\sigma \in \{0.03, 0.1\}$ and salt-and-pepper $p \in \{0.01, 0.05\}$), and spatial blur (Gaussian $\sigma \in \{1, 2\}$, defocus radius $r \in \{3, 7\}$, and motion kernel $L \in \{7, 21\}$). Each condition is applied independently; all other processing is identical to the standard inference pipeline.

Across all conditions and both subsets, CAM-VFD outperforms DeMamba by a consistent margin. Under heavier corruption at $CRF=32$, CAM-VFD leads DeMamba by 14.9% on SVD and 11.4% on CogVideo, achieving 83.9% and 91.6% accuracy while DeMamba achieves 69.0% and 80.2% respectively. CAM-VFD drops most under strong motion blur ($L=21$), where temporal cues are most directly damaged: SVD falls to 76.7% and CogVideo to 86.0%. This is the expected worst case because VideoMAE motion features are most sensitive to motion blur distortion, while CLIP and MiDaS features, which operate on individual frames, provide partial but incomplete compensation. Noise and lighting distortions produce the smallest degradation, reflecting the pre-trained backbones’ focus on abstract semantic rep-

Table 9: Signal degradation robustness: accuracy (%) of CAM-VFD and DeMamba [35] under identical compression, noise, and blur conditions on two GenVidBench subsets (CogVideo and SVD).

Subset	Method	Compression (H.264 CRF)				Noise				Blur					
		Base	18	28	32	Gaussian		Salt-Pepper		Gaussian		Defocus		Motion	
						$\sigma=0.03$	$\sigma=0.1$	$p=0.01$	$p=0.05$	$\sigma=1$	$\sigma=2$	$r=3$	$r=7$	$L=7$	$L=21$
CogVideo	DeMamba [35]	97.6	96.1	89.7	80.2	93.8	82.4	91.0	84.6	88.3	79.5	84.1	80.9	83.5	74.8
	CAM-VFD	99.7	99.2	96.8	91.6	98.0	90.8	95.1	91.4	95.9	98.5	93.2	90.7	91.8	86.0
SVD	DeMamba [35]	84.3	82.1	77.8	69.0	78.2	73.5	76.9	70.4	74.1	68.3	72.6	65.8	70.2	61.4
	CAM-VFD	90.2	89.8	88.4	83.9	89.3	85.7	88.4	81.2	87.5	81.2	85.7	78.5	83.0	76.7

Table 10: Robustness of CAM-VFD under photometric perturbations, including lighting (brightness, contrast) and color distortions (saturation, hue shift).

Subset	Lighting				Color Distortion					
	Base	$\Delta=0.05$	$\Delta=0.1$	$\alpha=0.7$	$\alpha=1.3$	$s=0.7$	$s=1.3$	$\Delta h=5^\circ$	$\Delta h=12^\circ$	
CogVideo	99.7	99.7	98.3	96.0	98.4	97.1	98.5	97.5	93.2	
SVD	90.2	90.2	89.8	87.5	86.6	89.0	88.4	88.4	86.6	

representations that are inherently insensitive to high-frequency or photometric perturbations.

CAM-VFD similarly exhibits negligible accuracy change under photometric perturbations (Table 10): brightness offsets ($\Delta \leq 0.1$), contrast scaling ($0.7 \leq \alpha \leq 1.3$), saturation shifts ($0.7 \leq s \leq 1.3$), and hue rotation ($\Delta h \leq 12^\circ$), with all photometric conditions maintaining accuracy above 86% on both subsets.

6.2 Adversarial Robustness

We evaluate the robustness of CAM-VFD under standard adversarial threat models using FGSM and PGD-20 attacks [53]. We apply FGSM (single-step) and PGD-20 (iterative) adversarial attacks with $\epsilon \in \{2/255, 4/255, 8/255\}$ defining the maximum perturbation magnitude applied to each pixel. As reported in Table 11, CAM-VFD exhibits relatively consistent robustness across increasing perturbation strengths, demonstrating strong robustness across both single-stream (appearance-only) and full-model attack settings. Under appearance attacks, performance decreases gradually from 99.74% in the clean setting to 84.17% under FGSM and 79.43% under the strongest PGD-20 attack. This is a direct consequence of the multimodal architecture: perturbing the appearance stream does not affect VideoMAE or MiDaS. Under the full-model attack, where perturbations are applied across all modalities, performance degradation remains moderate (82.31% and 77.68%). These results confirm the robustness of the proposed cross-attention fusion mechanism to both feature-level and joint multimodal attacks.

Table 11: Adversarial robustness under FGSM and PGD-20 attacks on the CogVideo subset of GenVidBench (clean accuracy: 99.74%).

Attack	ϵ	App.-only (%)	Full-model (%)
FGSM	2/255	96.44	95.22
FGSM	4/255	91.32	88.94
FGSM	8/255	84.17	82.31
PGD-20	4/255	88.66	85.42
PGD-20	8/255	79.43	77.68

7 Conclusion

Going beyond traditional facial manipulations to fabricate entire video scenes using AI-powered generation tools represents a direct and escalating threat to digital security: to the integrity of forensic evidence, to the authenticity of information, and to the trustworthiness of digital identity. Addressing this threat demands detection systems that are robust and generalizable. In this paper, we introduced *CAM-VFD*, a Cross-Attention Multimodal Video Forgery Detection framework for detecting fully AI-generated videos. The approach is based on the principle that cross-modal contradiction—systematic misalignment between appearance, geometric depth, and motion dynamics—is a more stable and generalisable forgery signal than any within-modality artifact. This design improves generalization to unseen generative models and enhances robustness under real-world distortions, including compression, noise, blur, and adversarial perturbations. Furthermore, our proposed Cross-Modal Attention Discrepancy (CMAD) analysis provides interpretability by quantifying the cross-modal inconsistency between real and fake videos.

Despite these advantages, CAM-VFD still exhibits limitations in scenarios where motion cues are weak or temporally ambiguous, such as near-static videos or extremely low-motion scenes, which reduce the discriminability of VideoMAE features. Moreover, the rapid evolution of synthetic video generators may pose future constraints. The proposed framework establishes multimodal cross-attention fusion as a dependable forensic strategy for AI-generated video detection, and provides a strong foundation for future work in which we aim to further explore adaptive modality and frame sampling to improve performance and robustness. Finally, integrating explainable AI (XAI) techniques could provide interpretable forensic evidence for model decisions, increasing transparency and trust in forensic verification systems.

References

- [1] A. Kaur, A. N. Hoshyar, V. Saikrishna, S. Firmin, and F. Xia, “Deepfake video detection: challenges and opportunities,” *Artificial Intelligence Review*, vol. 57, no. 6, p. 159, 2024.

- [2] Z. Akhtar, “Deepfakes generation and detection: A short survey,” *Journal of Imaging*, vol. 9, p. 18, 2023.
- [3] L. Guarnera, O. Giudice, and S. Battiato, “Deepfake detection by analyzing convolutional traces,” *Proceedings of the IEEE/CVF conference on computer vision and pattern recognition workshops*, pp. 666–667, 2020.
- [4] F. Matern, C. Riess, and M. Stamminger, “Exploiting visual artifacts to expose deepfakes and face manipulations,” in *2019 IEEE Winter Applications of Computer Vision Workshops (WACVW)*, 2019, pp. 83–92.
- [5] F. Becattini, C. Bisogni, V. Loia, C. Pero, and F. Hao, “Head pose estimation patterns as deepfake detectors,” *ACM Transactions on Multimedia Computing, Communications and Applications*, vol. 20, no. 11, pp. 1–24, 2024.
- [6] S. K. Datta, S. Jia, and S. Lyu, “Exposing lip-syncing deepfakes from mouth inconsistencies,” in *2024 IEEE International Conference on Multimedia and Expo (ICME)*. IEEE, 2024, pp. 1–6.
- [7] W. Liu, T. She, J. Liu, B. Li, D. Yao, and R. Wang, “Lips are lying: Spotting the temporal inconsistency between audio and visual in lip-syncing deepfakes,” *Advances in Neural Information Processing Systems*, vol. 37, pp. 91 131–91 155, 2024.
- [8] X. H. Nguyen, T. S. Tran, V. T. Le, K. D. Nguyen, and D.-T. Truong, “Learning spatio-temporal features to detect manipulated facial videos created by the deepfake techniques,” *Forensic Science International: Digital Investigation*, vol. 36, p. 301108, 2021. [Online]. Available: <https://www.sciencedirect.com/science/article/pii/S2666281721000020>
- [9] J. Bai, M. Lin, G. Cao, and Z. Lou, “Ai-generated video detection via spatial-temporal anomaly learning,” in *Chinese Conference on Pattern Recognition and Computer Vision (PRCV)*. Springer, 2024, pp. 460–470.
- [10] M. Bohacek and H. Farid, “Human action clips: Detecting ai-generated human motion,” *arXiv preprint arXiv:2412.00526*, 2024.
- [11] E. Prashnani, M. Goebel, and B. S. Manjunath, “Generalizable deepfake detection with phase-based motion analysis,” *IEEE Transactions on Image Processing*, vol. 34, pp. 100–112, 2025.
- [12] X. Wang, S. Zhang, H. Yuan, Z. Qing, B. Gong, Y. Zhang, Y. Shen, C. Gao, and N. Sang, “A recipe for scaling up text-to-video generation with text-free videos,” in *Proceedings of the IEEE/CVF Conference on Computer Vision and Pattern Recognition*, 2024, pp. 6572–6582.
- [13] Y. Hu, C. Luo, and Z. Chen, “Make it move: controllable image-to-video generation with text descriptions,” in *Proceedings of the IEEE/CVF Conference on Computer Vision and Pattern Recognition*, 2022, pp. 18 219–18 228.
- [14] Y. Li and S. Lyu, “Exposing deepfake videos by detecting face warping artifacts,” *arXiv preprint arXiv:1811.00656*, 2018.

- [15] J. Wang, Z. Wu, W. Ouyang, X. Han, J. Chen, Y.-G. Jiang, and S.-N. Li, “M2tr: Multi-modal multi-scale transformers for deepfake detection,” in *Proceedings of the 2022 International Conference on Multimedia Retrieval*, ser. ICMR '22. New York, NY, USA: Association for Computing Machinery, 2022, p. 615–623. [Online]. Available: <https://doi.org/10.1145/3512527.3531415>
- [16] M. Lomnitz, Z. Hampel-Arias, V. Sandesara, and S. Hu, “Multimodal approach for deepfake detection,” in *2020 IEEE Applied Imagery Pattern Recognition Workshop (AIPR)*, 2020, pp. 1–9.
- [17] A. Radford, J. W. Kim, C. Hallacy, A. Ramesh, G. Goh, S. Agarwal, G. Sastry, A. Askell, P. Mishkin, J. Clark *et al.*, “Learning transferable visual models from natural language supervision,” in *International conference on machine learning*. PmLR, 2021, pp. 8748–8763.
- [18] Z. Tong, Y. Song, J. Wang, and L. Wang, “Videomae: Masked autoencoders are data-efficient learners for self-supervised video pre-training,” *Advances in neural information processing systems*, vol. 35, pp. 10 078–10 093, 2022.
- [19] R. Ranftl, K. Lasinger, D. Hafner, K. Schindler, and V. Koltun, “Towards robust monocular depth estimation: Mixing datasets for zero-shot cross-dataset transfer,” *IEEE transactions on pattern analysis and machine intelligence*, vol. 44, no. 3, pp. 1623–1637, 2020.
- [20] R. Ranftl, A. Bochkovskiy, and V. Koltun, “Vision transformers for dense prediction,” in *Proceedings of the IEEE/CVF international conference on computer vision*, 2021, pp. 12 179–12 188.
- [21] B. Subburaj and R. Ragavendra, “Deepfake detection using spatio-temporal-structural anomaly learning and fuzzy system-based decision fusion,” *IEEE Access*, vol. 13, pp. 82 747–82 758, 2025.
- [22] C. Zhu, B. Zhang, Q. Yin, C. Yin, and W. Lu, “Deepfake detection via inter-frame inconsistency recomposition and enhancement,” *Pattern Recognition*, vol. 147, p. 110077, 2024. [Online]. Available: <https://www.sciencedirect.com/science/article/pii/S0031320323007744>
- [23] T. Zhang, G. Li, Y. Xiao, H. Tian, and Y. Cao, “Enhanced deepfake detection via dynamic data augmentation and spatiotemporal attention,” *Vis. Comput.*, vol. 42, no. 1, Dec. 2025. [Online]. Available: <https://doi.org/10.1007/s00371-025-04199-8>
- [24] D. Nguyen, M. Astrid, A. Kacem, E. Ghorbel, and D. Aouada, “Vulnerability-aware spatio-temporal learning for generalizable deepfake video detection,” 2025. [Online]. Available: <https://arxiv.org/abs/2501.01184>
- [25] H. Wang, Z. Liu, and S. Wang, “Exploiting complementary dynamic incoherence for deepfake video detection,” *IEEE Transactions on Circuits and Systems for Video Technology*, vol. 33, no. 8, pp. 4027–4040, 2023.

- [26] Z. Gu, Y. Chen, T. Yao, S. Ding, J. Li, and L. Ma, “Delving into the local: Dynamic inconsistency learning for deepfake video detection,” *Proceedings of the AAAI Conference on Artificial Intelligence*, vol. 36, no. 1, pp. 744–752, Jun. 2022. [Online]. Available: <https://ojs.aaai.org/index.php/AAAI/article/view/19955>
- [27] T. Oorloff, S. Koppiseti, N. Bonettini, D. Solanki, B. Colman, Y. Yacoob, A. Shahriyari, and G. Bharaj, “Avff: Audio-visual feature fusion for video deepfake detection,” in *Proceedings of the IEEE/CVF Conference on Computer Vision and Pattern Recognition*, 2024, pp. 27 102–27 112.
- [28] C. Chang, Z. Liu, X. Lyu, and X. Qi, “What matters in detecting ai-generated videos like sora?” *arXiv preprint arXiv:2406.19568*, 2024.
- [29] Y. Du, Z. Wang, Y. Luo, C. Piao, Z. Yan, H. Li, and L. Yuan, “Cad: A general multimodal framework for video deepfake detection via cross-modal alignment and distillation,” 2025. [Online]. Available: <https://arxiv.org/abs/2505.15233>
- [30] L. Lv, T. Wang, M. Huang, R. Liu, and Y. Wang, “A spatial-frequency aware multi-scale fusion network for real-time deepfake detection,” 2025. [Online]. Available: <https://arxiv.org/abs/2508.20449>
- [31] L. Zhang, B. Liu, Q. Chu, and N. Yu, “Multimodal consistency-driven deepfake detection,” in *Image and Graphics: 13th International Conference, ICIG 2025, Xuzhou, China, October 31 – November 2, 2025, Proceedings, Part II*. Berlin, Heidelberg: Springer-Verlag, 2025, p. 293–303. [Online]. Available: https://doi.org/10.1007/978-981-95-3393-0_24
- [32] Z. Wu, C. Xiong, C. Ma, R. Socher, and L. S. Davis, “Adaframe: Adaptive frame selection for fast video recognition,” *CoRR*, vol. abs/1811.12432, 2018. [Online]. Available: <http://arxiv.org/abs/1811.12432>
- [33] A. Paszke, S. Gross, F. Massa, A. Lerer, J. Bradbury, G. Chanan, T. Killeen, Z. Lin, N. Gimelshein, L. Antiga, A. Desmaison, A. Köpf, E. Z. Yang, Z. DeVito, M. Raison, A. Tejani, S. Chilamkurthy, B. Steiner, L. Fang, J. Bai, and S. Chintala, “Pytorch: An imperative style, high-performance deep learning library,” *CoRR*, vol. abs/1912.01703, 2019. [Online]. Available: <http://arxiv.org/abs/1912.01703>
- [34] Z. Ni, Q. Yan, M. Huang, T. Yuan, Y. Tang, H. Hu, X. Chen, and Y. Wang, “Genvidbench: A challenging benchmark for detecting ai-generated video,” 2025. [Online]. Available: <https://arxiv.org/abs/2501.11340>
- [35] H. Chen, Y. Hong, Z. Huang, Z. Xu, Z. Gu, Y. Li, J. Lan, H. Zhu, J. Zhang, W. Wang, and H. Li, “Demamba: Ai-generated video detection on million-scale genvideo benchmark,” 2024. [Online]. Available: <https://arxiv.org/abs/2405.19707>
- [36] J. Carreira and A. Zisserman, “Quo vadis, action recognition? a new model and the kinetics dataset,” 2018. [Online]. Available: <https://arxiv.org/abs/1705.07750>
- [37] C. Feichtenhofer, H. Fan, J. Malik, and K. He, “Slowfast networks for video recognition,” 2019. [Online]. Available: <https://arxiv.org/abs/1812.03982>

- [38] C. Yang, Y. Xu, J. Shi, B. Dai, and B. Zhou, “Temporal pyramid network for action recognition,” 2020. [Online]. Available: <https://arxiv.org/abs/2004.03548>
- [39] H. Shao, S. Qian, and Y. Liu, “Temporal interlacing network,” *Proceedings of the AAAI Conference on Artificial Intelligence*, vol. 34, no. 07, pp. 11 966–11 973, Apr. 2020. [Online]. Available: <https://ojs.aaai.org/index.php/AAAI/article/view/6872>
- [40] C. Feichtenhofer, “X3d: Expanding architectures for efficient video recognition,” 2020. [Online]. Available: <https://arxiv.org/abs/2004.04730>
- [41] B. Zhou, A. Andonian, A. Oliva, and A. Torralba, “Temporal relational reasoning in videos,” 2018. [Online]. Available: <https://arxiv.org/abs/1711.08496>
- [42] J. Lin, C. Gan, and S. Han, “Tsm: Temporal shift module for efficient video understanding,” 2019. [Online]. Available: <https://arxiv.org/abs/1811.08383>
- [43] K. Li, Y. Wang, Y. He, Y. Li, Y. Wang, L. Wang, and Y. Qiao, “Uniformerv2: Spatiotemporal learning by arming image vits with video uniformer,” 2022. [Online]. Available: <https://arxiv.org/abs/2211.09552>
- [44] G. Bertasius, H. Wang, and L. Torresani, “Is space-time attention all you need for video understanding?” 2021. [Online]. Available: <https://arxiv.org/abs/2102.05095>
- [45] Z. Liu, J. Ning, Y. Cao, Y. Wei, Z. Zhang, S. Lin, and H. Hu, “Video swin transformer,” 2021. [Online]. Available: <https://arxiv.org/abs/2106.13230>
- [46] Y. Li, C.-Y. Wu, H. Fan, K. Mangalam, B. Xiong, J. Malik, and C. Feichtenhofer, “Mvitv2: Improved multiscale vision transformers for classification and detection,” 2022. [Online]. Available: <https://arxiv.org/abs/2112.01526>
- [47] S. Zhang, Z. Lian, J. Yang, D. Li, G. Pang, F. Liu, B. Han, S. Li, and M. Tan, “Physics-driven spatiotemporal modeling for ai-generated video detection,” 2025. [Online]. Available: <https://arxiv.org/abs/2510.08073>
- [48] S. Du, X. Luo, D. P. O’Regan, and C. Qin, “Stil: Semi-supervised tabular-image learning for comprehensive task-relevant information exploration in multimodal classification,” 2025. [Online]. Available: <https://arxiv.org/abs/2503.06277>
- [49] C. Tan, H. Liu, Y. Zhao, S. Wei, G. Gu, P. Liu, and Y. Wei, “Rethinking the up-sampling operations in cnn-based generative network for generalizable deepfake detection,” 2023. [Online]. Available: <https://arxiv.org/abs/2312.10461>
- [50] Y. Xu, J. Liang, G. Jia, Z. Yang, Y. Zhang, and R. He, “Tall: Thumbnail layout for deepfake video detection,” 2024. [Online]. Available: <https://arxiv.org/abs/2307.07494>
- [51] Student, “The probable error of a mean,” *Biometrika*, pp. 1–25, 1908.
- [52] J. Cohen, “Statistical power analysis for the behavioral sciences,” 1988.
- [53] W. Villegas-Ch, A. Jaramillo-Alcázar, and S. Luján-Mora, “Evaluating the robustness of deep learning models against adversarial attacks: An analysis with fgsm, pgd and

cw,” *Big Data and Cognitive Computing*, vol. 8, no. 1, 2024. [Online]. Available: <https://www.mdpi.com/2504-2289/8/1/8>